Journal of Solid State Chemistry 186 (2012) 76–80

Contents lists available at SciVerse ScienceDirect

Journal of Solid State Chemistry

journal homepage: www.elsevier.com/locate/jssc

CuO–ZnO heterometallic hollow spheres: Morphology and defect structure

Xuemin Shi, Xuzhuang Yang, Xiaojun Gu, Haiquan Su *

Inner Mongolia Key Laboratory of Coal Chemistry, School of Chemistry and Chemical Engineering, Inner Mongolia University, Hohhot 010021, PR China

ARTICLE INFO

Article history:
Received 24 August 2011
Received in revised form
16 November 2011
Accepted 27 November 2011
Available online 4 December 2011

Keywords:
CuO–ZnO
Hollow structure
Defect
Carbon spheres

ABSTRACT

The Cu–ZnO hollow spheres, where CuO nanocrystals were dispersed in the shell of ZnO nanoparticals, were synthesized by using highly uniform and monodispersed Cu-embedded carbon spheres as sacrificial templates via a simple route under hydrothermal conditions. The morphology and structure of the spheres were characterized by FTIR, XRD, SEM, TEM and N_2 adsorption–desorption. It was suggested that the OH and C=O groups in the surface of the Cu-embedded carbon spheres facilitated the adsorption of Zn^{2+} in the aqueous solution, giving rise to the final CuO–ZnO hollow structure after these Zn^{2+}-adsorbed spheres were calcined in air. Moreover, the photoluminescence (PL) study showed that the as-prepared CuO–ZnO hollow spheres and the annealed counterpart exhibited strong and dramatically weakened emissions, respectively. This remarkably different photoluminescent behavior afforded the evidence regarding the oxygen vacancy defects in the CuO–ZnO hollow spheres.

1. Introduction

In the field of materials science, ZnO is a well-known n-type ionic semiconductor originating from the intrinsic defects, and its defect density is usually exploited for explaining the superior properties [1,2]. In solid state materials, since the defects are closely related to their physiochemical properties, a variety of theory and experiment methods have been explored to study this interesting phenomenon [1–7]. Photoluminescence (PL) is the most useful technique for identifying the defect in semiconductors. In the PL spectra of ZnO, typically there are emission bands in the ultraviolet (UV) and visible regions. The UV emission is usually attributed to the band-edge transition or the excited combination [8], while the emissions in the visible regions are universally considered to be associated with the intrinsic or extrinsic defects in ZnO [9,10]. However, some reports show that their blue emissions result from the oxygen vacancy-related defect [11–13]. In order to identify the origin of the defect emissions, it is necessary to suppress the defect emission either by post-fabrication treatment or by varying the fabrication conditions [7].

Doping of ZnO with other elements often affects the defect of ZnO, resulting in unique electrical, optical and magnetic properties, which, therefore, has attracted a lot of research interests [14–16]. The emission spectra of Cu-doped ZnO extend from the ultraviolet to the infrared region depending on the concentration of copper, defects in ZnO, and excitation conditions [17–19]. In addition, some results show that the morphology of ZnO plays an important role in its chemical and physical properties, such as the defects [19,20]. As is well known, hollow structures exhibit a lower density, higher surface area, and distinct optical property, having promising perspectives in optical, electronic, magnetic, catalytic, acoustic and sensing devices [21–24]. Recently, many efforts have been made to prepare hollow ZnO structures using different methods [25–28]. Using colloidal carbon spheres as template has been proven to be a successful method to prepare metal oxides hollow structures, including ZnO hollow spheres [28–30]. But the low yield of carbon spheres retards the development of this method.

Herein a simple route of the synthesis of CuO–ZnO heterometallic hollow spheres using carbon spheres as sacrificed templates was reported. And the growth model of the heterometallic hollow spheres was also explored. Furthermore, the defect structure was identified by post-fabrication treatment via the PL technique. The relationship between morphologies and different synthetic parameters were studied as well.

2. Experimental

2.1. Synthesis of the carbon spheres

Cu-embedded carbon spheres (C-CS) were prepared by the hydrothermal method. First, 6.76 g glucose was dissolved in 70 ml deionized water to form a clear solution, followed by adding 5 ml copper nitrate water solution of a certain concentration (0.02 M, 0.15 M, 0.20 M). Then, the mixture was transferred into a 125 mL Teflon-lined autoclave and maintained at 160 °C for 12 h. The obtained suspension was centrifuged, washed, and re-dispersed

* Corresponding author. Fax: +86 471 4992979.
E-mail address: haiquansu@yahoo.com (H. Su).

0022-4596/$ - see front matter © 2011 Elsevier Inc. All rights reserved.
doi:10.1016/j.jssc.2011.11.045

in water and ethanol by three cycles, and then dried at 80 °C in air. The samples were labeled as C-CS-0.02, C-CS-0.15 and C-CS-0.20, respectively, corresponding to the concentration of copper.

The pure carbon spheres (CS) were synthesized by the same method without the addition of copper nitrate solutions [29].

2.2. Synthesis of the CuO–ZnO hollow spheres

1 g as-prepared C-CS was dispersed in 50 mL $Zn(CH_3COO)_2$ (0.5 M) solution, followed by ultrasonicating for 60 min. The obtained suspension was aged for 24 h, and then centrifuged and washed with deionized water three times. Finally, the obtained solids were dried in air at 80 °C for 12 h, and calcined in air at 500 °C for 2 h. The samples using C-CS-0.02, C-CS-0.15 and C-CS-0.20 as template were marked as HS-0.02, HS-0.15 and HS-0.20, respectively.

2.3. Characterization

An Inductively Coupled Plasma Optical Emission Spectrometer (ICP-OES, OPTIMA7000DV) was used to investigate the copper content in the samples, which was 2.22 wt%, 23.90 wt% and 25.92 wt% for C-CS-0.02, C-CS-0.15 and C-CS-0.20, respectively. The functional groups on the surface of samples were studied by an infrared spectrophotometer (NEXUS-670) with KBr pellet. The phases of the samples were characterized by an X-ray diffractometer (XRD, Rigaku DMAX-2400), operated at 36 kV and 20 mA using Cu$K\alpha$ radiation at a scan rate of $0.03^\circ\ s^{-1}$ through the 2θ–range from 10° to 80°. The morphology and structure of the samples were investigated by the scanning electron microscopy (SEM, S-3400N) and high-resolution transmission electron microscopy (HRTEM, JEM-2010 (JEOL)). N_2 adsorption–desorption isotherms of the samples were measured at −196 °C on a Micromeritics ASAP2020 equipment. Pore size distributions were obtained by applying the BJH formalism to the adsorption branch of the isotherms. The photoluminescence of samples was recorded on a FLS920 Fluorescence spectrophotometer at room temperature.

3. Results and discussion

3.1. Characterization of carbon spheres

To obtain detailed information about the microstructure and morphology of the synthesized carbon templates, SEM was carried out. The images are shown in Fig. 1. Apparently, the carbon spheres were quite uniform and monodispersed. The diameter of the carbon spheres was about 230 nm, while the diameter of the copper embedded carbon spheres (C-CS-0.02) was about 1500 nm, 6.5 times as large as carbon spheres, suggesting that the addition of copper ions accelerates the growth of sphere. From Fig. 1b–d, it can be seen that the average diameters of C-CS-0.15 and C-CS-0.20 were about 2000 nm, larger than the diameter of C-CS-0.02, indicating the size of the spheres increase with the growth of the concentration of embedded Cu ions.

For the conventional synthesis of the carbon spheres, the yield of CS was very low (about 2.0%). In our experiments, when adding copper ions, the size of C-CS was greatly enhanced, and the product was easy to separate from the solution, resulting in a much higher yield (Table 1). Besides, the whole process including the fabrication of the hollow spheres was carried out under aqueous conditions without using any organic solvent or etching agent.

The FT-IR spectra (Fig. 2) were used to identify the functional groups of CS and C-CS samples. The bands at 1700 and 1640 cm^{-1} were attributed to C=O and C=C vibrations, while the bands at 3418 cm^{-1} was corresponded to the OH stretching vibration, implying the existence of a large number of hydroxyl groups on the surface of samples. The hydrophilic surfaces functionalized with OH and C=O groups are beneficial to the growth of ZnO species on them [31].

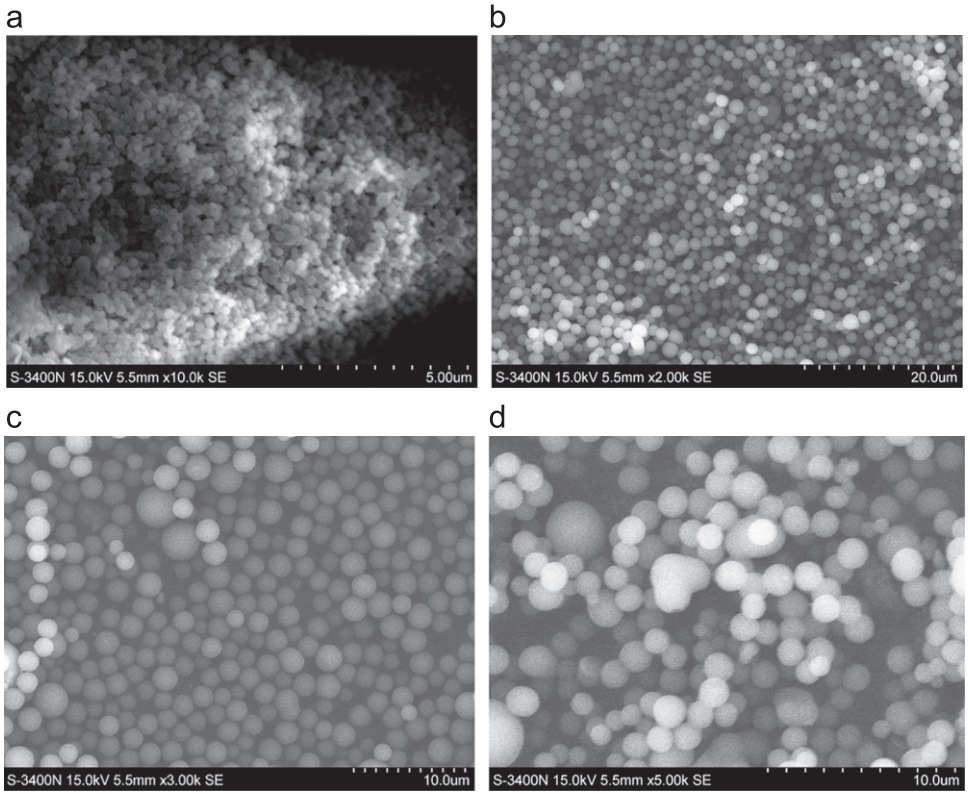

Fig. 1. SEM images of the samples (a) CS, (b) C-CS-0.02, (c) C-CS-0.15 and (d) C-CS-0.20.

Table 1
Separation condition and production of CS and C-CS.

Sample	Centrifugation speed (rpm)	Centrifugation time (min)	Yield (%)
CS	10,000	30	2.0
C-CS-0.02	3000	15	38.2
C-CS-0.15	3000	15	41.5
C-CS-0.20	3000	15	43.0

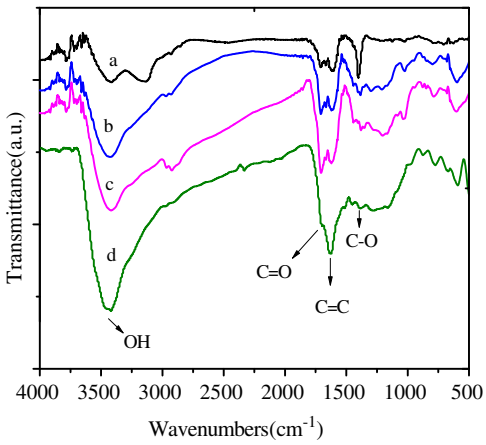

Fig. 2. FT-IR spectra of (a) CS, (b) C-CS-0.02, (c) C-CS-0.15 and (d) C-CS-0.20.

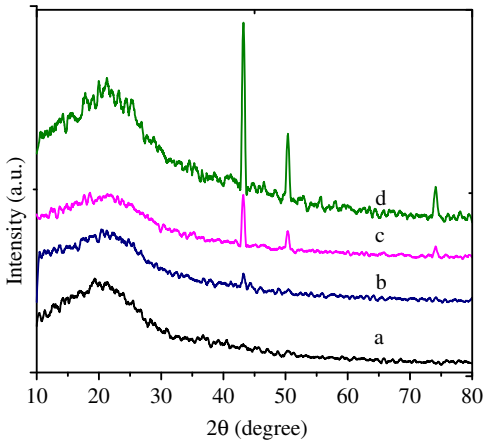

Fig. 3. XRD patterns of (a) CS, (b) C-CS-0.02, (c) C-CS-0.15 and (d) C-CS-0.20.

Fig. 3 shows XRD patterns of C-CS samples. The broad peak at about 20° of the 2θ in each pattern was ascribed to the amorphous carbon diffraction. The peaks at 43.20°, 50.34° and 74.11° corresponded to the Cu diffractions of (1 1 1), (2 0 0) and (2 2 0), respectively (JCPDS 65-9026). The Cu diffractions intensified with increasing copper dose in samples.

3.2. Morphology and composition of CuO–ZnO hollow spheres

Fig. 4 shows the XRD patterns of the CuO–ZnO samples. The peaks at 35.38°, 38.71° and 48.78° of the 2θ were attributed to the CuO diffractions of (0 0 2), (1 1 1) and (−2 0 2), respectively. The other diffraction peaks matched the standard data for a hexagonal ZnO wurtzite structure (JCPDS 36-1451), which demonstrates that the added Cu ions have no effects on the crystal structure of ZnO. No CuO diffraction peaks were observed when the Cu

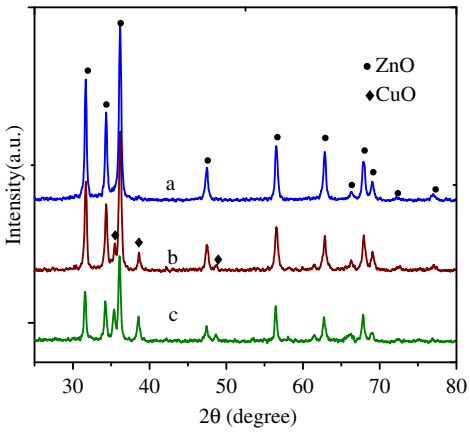

Fig. 4. XRD patterns of (a) HS-0.02, (b) HS-0.15 and (c) HS-0.20.

Table 2
The crystalline sizes of hollow spheres.

Sample	ZnO (1 0 0) crystalline size (nm)	CuO (1 1 1) crystalline size (nm)
C-CS-0.02	32.0	
C-CS-0.15	32.2	26.5
C-CS-0.20	33.7	34.1

content is 2.22 wt%. This phenomenon may be caused by that CuO content of HS-0.02 is below the detection limits of the XRD instrument or the CuO species are dispersed well on the surface of ZnO nanoparticles. With the growth of copper content, the CuO diffraction peaks became more obvious and stronger. The average crystallite sizes of hollow samples can be calculated by applying the Debye–Scherrer formula on the ZnO (1 0 0) diffraction peaks and the CuO (1 1 1) (Table 2). The results show that the size of ZnO(1 0 0) is about 32 nm, and the size of CuO (1 1 1) in HS-0.15 and HS-0.20 are 26 nm and 34 nm, respectively.

The SEM and TEM images of the CuO–ZnO hollow spheres are shown in Fig. 5. The hollow structures were observed obviously in both SEM and TEM images. SEM images of HS-0.02 (Fig. 5a and b) show that the outer surface of the hollow spheres was rough and stacked with small nanoparticles standing out of the surface. Furthermore, irregular pores, which result from the pile of nanoparticles, could be observed on the surface of those spheres. The diameter of the HS-0.02 hollow spheres was about 550 nm (45 nm in shell thickness), smaller than that of its template precursor C-CS-0.02 (1500 nm). The shrinkage could be attributed to the decarbonization and dehydration of the carbon template.

Fig. 5d and f are the HRTEM images of HS-0.02 and HS-0.15. The lattices indicated that the shell was composed of a large amount of ZnO nanocrystals and a small amount of CuO nanocrystals. The HRTEM investigation indicates that CuO nanocrystals were dispersed among ZnO nanocrystals forming the shell of the hollow sphere. The N_2 adsorption–desorption method was also employed to confirm the porosity of CuO–ZnO hollow spheres. Fig. 6a depicts the N_2 adsorption–desorption isotherms of HS-0.02, indicating the existence of pores on the shell of the ZnO hollow spheres. The isotherm shows a distinct hysteresis loop observed in the P/P^o range of 0.80–0.95, which suggested the existence of uniform pores with larger size in this sample and the extension of pore size distribution to the macropore range. The BET surface area is as high as 12.90 m^2/g calculated from the data in the P/P^o region of 0.05–0.35. Fig. 6b shows the BJH pore-size distribution curve of HS-0.02, exhibiting pore sizes focusing in the range of

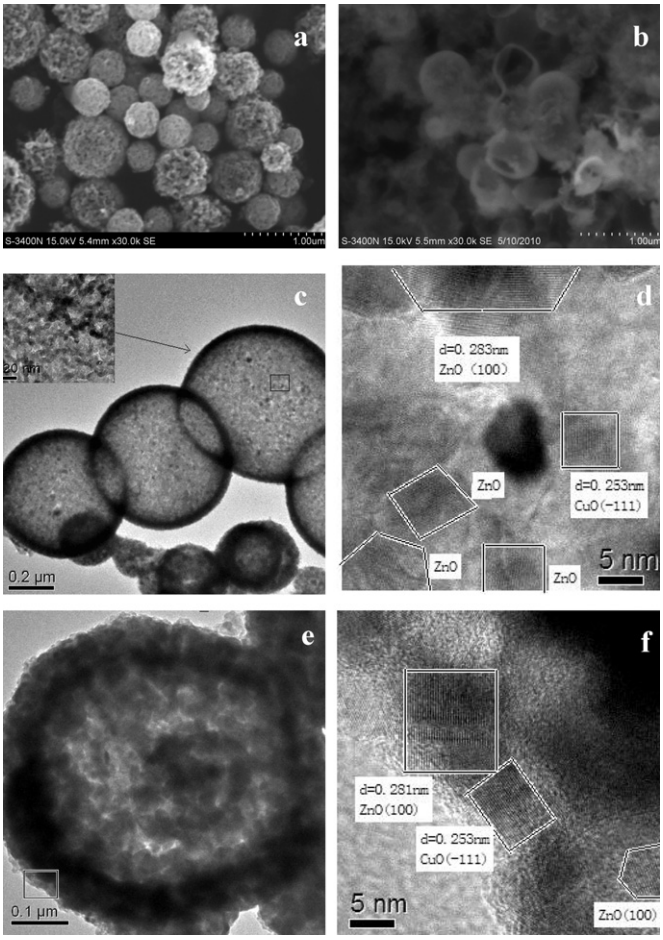

Fig. 5. SEM images of (a, b) HS-0.02 and TEM and HRTEM images of (c, d) HS-0.02 and (e, f) HS-0.15.

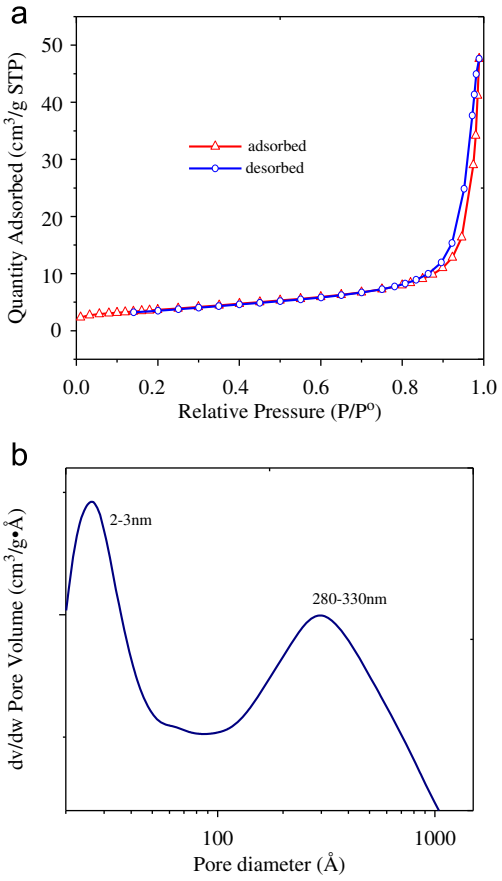

Fig. 6. (a) Nitrogen adsorption–desorption isotherms and (b) pore size distribution curve of HS-0.02.

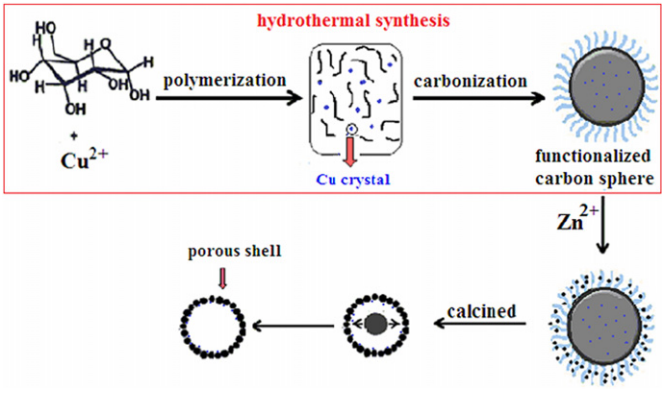

Fig. 7. Schematic illustration of the formation and morphology evolution of the hollow heterometallic sphere.

2–3 nm and 280–320 nm with a bimodal structure. The mesopores originated from the interstices among the small nanoparticles of the shell, while the macropores resulted from the void among the piled hollow spheres, which were in good agreement with the SEM and TEM observations of the hollow ZnO spheres.

3.3. The formation mechanism of the CuO–ZnO hollow spheres

Based on the experimental results, a possible growth schematic diagram for the CuO–ZnO hollow spheres was proposed, as shown in Fig. 7. First, Cu^{2+} was reduced into Cu crystals by carbonyl group of glucose under hydrothermal condition. Then, the Cu crystals performed as seeds, on which glucose dehydrated to carbon structures which fabricated the carbon spheres mixed with Cu crystals. So at the same synthesis conditions, the size of the copper embedded carbon spheres was larger than that of the carbon spheres, as was proved by SEM.

Since the surface of the carbon spheres was full of OH and C=O groups, and was negative charged [28,29], it was hydrophilic and facile to absorb Zn^{2+}. When the spheres absorbed Zn^{2+} were calcined in air, ZnO nanocrystals formed on the shell of the sphere and the carbon core was removed by the oxidation of carbon into CO_2 simultaneously, CuO nanocrystals formed and dispersed into the shell.

3.4. Optical property and defects of the CuO–ZnO hollow spheres

The optical properties of the obtained samples were investigated by PL spectroscopy. In the PL spectra of the three CuO–ZnO hollows (Fig. 8a), there is a blue emission caused by oxygen vacancies at 452 nm (2.74 eV), which is very infrequent [11–13]. Oxygen vacancies can produce a donor level locating below the conduction band about 0.3–0.5 eV [30], and the energy interval (2.8 eV) from this donor level to the top of the valence was more close to the emission at 2.74 eV in our experiment. To verify this assumption, we annealed the sample at 600 °C for 2 h under oxygen atmosphere. The PL spectrum of the annealed sample exhibits an obvious weakening on the emission intensity of the blue luminescence (Fig. 8b). After annealing in oxygen atmosphere, the density of the oxygen vacancies in the sample decreased because of the further combination of the oxygen with the oxygen vacancies. Consequently, the reduced density of the defects results

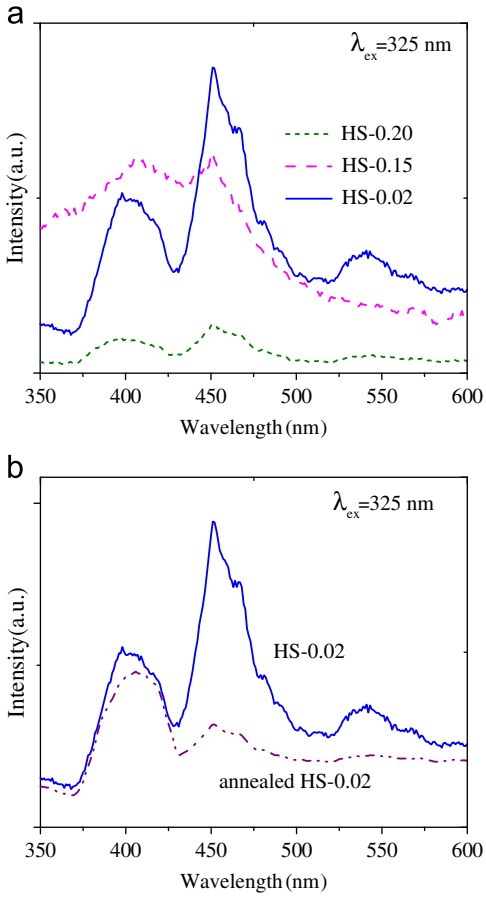

Fig. 8. Photoluminescence spectra of (a) CuO–ZnO samples with different Cu-doped concentrations and (b) HS-0.02 before and after annealed.

in the lessening of the blue PL emission intensity. Furthermore, there is a broad violet emission at 400 nm, which is caused by both the near band-edge emission and the electron transfer from a shallow donor of Cu^{2+} ($^2T_2$) to a valence band [8,31].

Concerning more details, the intensity of both the violet emission and the blue emission depend strongly on Cu concentration. In the sample of 23.5 wt% Cu-doped ZnO (HS-0.15), abundant Cu atoms existed as interstitials that share the oxygen atoms with Zn atoms and hence decrease the defects of oxygen vacancies, leading to the quenching of blue emission and the enhancement of violet emission. In general, there are some nonradiative recombination processes, especially the Auger process which depends on the concentration of doping atom in ZnO [32]. In our samples, when the Cu doping concentration further increases, the Auger process becomes predominant, resulting in the dramatical declines of all the emission intensity. Interestingly, a literature [33] reported the PL data for pure ZnO hollow spheres. There are a strong UV emission centered at around 400 nm and a weak emission centered at 466 nm in pure ZnO hollow spheres PL spectra. Compared to the above data with our results, it can be found that the addition of copper can affect the vacancies in ZnO hollow spheres.

On the basis of above discussion, it can be confirmed that there are enormous oxygen vacancies in CuO–ZnO hollow spheres (especially in HS-0.02), and these defects might be beneficial to their properties such as photocatalytic activity.

4. Conclusion

In summary, CuO–ZnO hollow spheres based on Cu-embedded carbon spheres with a high yield have been successfully prepared via a simple route under hydrothermal conditions. For the obtained hollow spheres, CuO nanocrystals were highly dispersed in the shell of ZnO nanoparticals, and different size and shell thicknesses of hollow spheres could be obtained by adjusting the concentration of copper in carbon sphere template. More importantly, our study afforded the evidence regarding the oxygen vacancy defects in ZnO semiconductor materials through PL spectra. The synthetic approach and the unique defect and bimodal pore structures might be applicable to preparing other types of materials with novel hollow structures and using as potential photocatalysts and gas sensors.

Acknowledgment

This work was supported by Preliminary 973 Project (no. 2009CB226112).

References

[1] Q. Kuang, Z.Y. Jiang, Z.X. Xie, S.C. Lin, Z.W. Lin, S.Y. Xie, R.B. Huang, L.S. Zheng, J. Am. Chem. Soc. 127 (2005) 11777–11784.
[2] Y. Zhang, J.Q. Xu, Q. Xiang, H. Li, Q.Y. Pan, P.C. Xu, J. Phys. Chem. C 113 (2009) 3430–3435.
[3] J.J. Schneider, R.C. Hoffmann, J. Engstler, A. Klyszcz, E. Erdem, P. Jakes, R.A. Eichel, L. Pitta Bauermann, J. Bill, Chem. Mater. 22 (2010) 2203–2212.
[4] D.S. Bohle, C.J. Spina, J. Am. Chem. Soc. 131 (2009) 4397–4404.
[5] B.H. Lin, W.R. Liu, S. Yang, C.C. Kuo, C.H. Hsu, W.F. Hsieh, W.C. Lee, Y.J. Lee, M. Hong, J. Kwo, Cryst. Growth Des. 11 (2011) 2846–2851.
[6] J.J. Cole, X.Y. Wang, R.J. Knuesel, H.O. Jacobs, Nano Lett. 8 (2008) 1477–1481.
[7] V. Ischenko, S. Polarz, D. Grote, V. Stavarache, K. Fink, M. Driess, Adv. Funct. Mater. 15 (2005) 1945–1954.
[8] X.N. Wang, H.J. Zhu, Y.M. Xu, H. Wang, Y. Tao, S.K. Hark, X.D. Xiao, Q. Li, ACS Nano 4 (2010) 3302–3308.
[9] D. Zhao, C. Andreazza, P. Andreazza, J. Ma, Y. Liu, D. Shen, Chem. Phys. Lett. 399 (2004) 522–526.
[10] A.B. Djurisic, Y.H. Leung, Small 2 (2006) 944–961.
[11] D.H. Liu, L. Liao, J.C. Li, H.X. Guo, Q. Fu, Mater. Sci. Eng. B 121 (2005) 77–80.
[12] Z. Chen, N. Wu, Z. Shan, M. Zhao, S. Li, C.B. Jiang, M.K. Chyu, S.X. Mao, Scr. Mater. 52 (2005) 63–67.
[13] Z.Y. Xue, D.H. Zhang, Q.P. Wang, J.H. Wang, Appl. Surf. Sci. 195 (2002) 126–129.
[14] J.Z. Kong, A.D. Li, H.F. Zhai, Y.P. Gong, H. Li, D. Wu, J. Solid State Chem. 182 (2009) 2061–2067.
[15] T. Gao, Q.H. Li, T.H. Wang, Chem. Mater. 17 (2005) 887–892.
[16] A.A. Khassin, V.V. Pelipenko, T.P. Minyukova, V.I. Zaikovskii, D.I. Kochubey, T.M. Yurieva, Catal. Today 112 (2006) 143–147.
[17] R. Viswanatha, S. Chakraborty, S. Basu, D.D. Sarma, J. Phys. Chem. B 110 (2006) 22310–22312.
[18] S. Eustis, D.C. Meier, M.R. Beversluis, B. Nikoobakht, ACS Nano 2 (2008) 368–376.
[19] Z. Zhang, J.B. Yi, J. Ding, L.M. Wong, H.L. Seng, S.J. Wang, J.G. Tao, G.P. Li, G.Z. Xing, T.C. Sum, C.H.A. Huan, T. Wu, J. Phys. Chem. C 112 (2008) 9579–9585.
[20] S.L. Wang, X. Jia, P. Jiang, H. Fang, W.H. Tang, J. Alloys Compd. 502 (2010) 118–122.
[21] H.Z. Wang, J.B. Liang, H. Fan, B.J. Xi, M.F. Zhang, S.L. Xiong, Y.C. Zhu, Y.T. Qian, J. Solid State Chem. 181 (2008) 122–129.
[22] S.W. Kim, M. Kim, W.Y. Lee, T. Hyeon, J. Am. Chem. Soc. 124 (2002) 7642–7643.
[23] H. Li, J. Liu, S.H. Xie, M.H. Qiao, W.L. Dai, Y.F. Lu, H.X. Li, Adv. Funct. Mater. 18 (2008) 3235–3241.
[24] Z.Y. Jiang, Z.X. Xie, X.H. Zhang, S.C. Lin, T. Xu, S.Y. Xie, R.B. Huang, L.S. Zheng, Adv. Mater. 16 (2004) 904–907.
[25] Q.Y. Li, W.L. Chen, M.L. Ju, L. Liu, E.B. Wang, J. Solid State Chem. 184 (2011) 1373–1380.
[26] P.X. Gao, Z.L. Wang, J. Am. Chem. Soc. 125 (2003) 11299–11305.
[27] Q.Y. Li, E.B. Wang, S.H. Li, C.L. Wang, C.G. Tian, G.Y. Sun, J.M. Gu, R. Xu, J. Solid State Chem. 182 (2009) 1149–1155.
[28] X.M. Sun, Y.D. Li, Angew. Chem. Int. Ed. 43 (2004) 3827–3831.
[29] X.M. Sun, Y.D. Li, Angew. Chem. Int. Ed. 43 (2004) 597–601.
[30] J.F. Cordaro, Y. Shim, J.E. May, J. Appl. Phys. 60 (1986) 4186–4190.
[31] C.X. Xu, X.W. Sun, X.H. Zhang, L. Ke, S.J. Chua, Nanotechnology 15 (2004) 856–861.
[32] X.B. Wang, C. Song, K.W. Geng, F. Zeng, F. Pan, Appl. Surf. Sci. 253 (2007) 6905–6909.
[33] J. Zhou, D. Wu, H. Guo, N. Liu, Y. Xiao, K.i Jiang, Mater. Sci. Eng. B 172 (2010) 96–100.